Arab J Geosci (2016) 9:413
DOI 10.1007/s12517-016-2429-3

ORIGINAL PAPER

Seismic spectrograms of an anelastic layer with different source-receivers configurations

Ayman N. Qadrouh[1,2] · José M. Carcione[3] · Ahmed M. A. Salim[1] · Zuhar Zahir Tuan Harith[4]

Received: 13 May 2015 / Accepted: 9 March 2016
© Saudi Society for Geosciences 2016

Abstract Thin and relatively thin anelastic layers (compared to the signal wavelength) generally represent hydrocarbon reservoirs, where the rock is a sandstone or a source rock saturated with brine, oil and gas. The study of the seismic response of these layers is important to detect the hydrocarbons on the basis of the reflection and transmission coefficients and the wave velocity and attenuation properties. Different seismic experiments (source-receiver configurations) can provide useful information to characterise its properties. In this work, we consider varying thicknesses and Q values of the layer and analyse the reflection and transmission coefficients. Moreover, we obtain spectrograms of surface seismic profiles and vertical and horizontal well profiles (VSP and HSP, respectively) to analyse their frequency content with offset due to variations of the attenuation properties of the layer. In addition, we compare the effects due to NMO stretching and intrinsic attenuation related to the low-frequency shadows (LFS) observed in real data after stacking, since LFS can have several causes. Ambiguity is present in this case, indicating that non-stretch NMO is required, otherwise an offset mute of the data may remove useful information regarding the intrinsic (physical) loss.

Keywords Layer · Attenuation · Spectrogram · Scattering coefficients · NMO stretch

✉ Ayman N. Qadrouh
aqadrouh@kacst.edu.sa

José M. Carcione
jcarcione@inogs.it

[1] Universiti Teknologi PETRONAS, Seri Iskandar 31750 Perak, Malaysia

[2] SAC - KACST, PO Box 6086, Riyadh 11442, Saudi Arabia

[3] Istituto Nazionale di Oceanografia e di Geofisica Sperimentale (OGS), Borgo Grotta Gigante 42c, 34010 Sgonico, Trieste, Italy

[4] Institute of Petroleum Engineering, Heriot-Watt University Malaysia, Level 2, Menara PjH, No. 2 Jalan Tun Abdul Razak, Precinct 2, 62100 Putrajaya, Malaysia

Introduction

Seismic attenuation can be used to obtain useful information about the presence of liquids and gas in the underground. In particular, hydrocarbon reservoirs in the form of thin layers have a low seismic quality factor due to wave-loss mechanisms. The main one in porous rocks is mesoscopic loss by wave-induced fluid flow (Müller et al. 2010; Carcione and Picotti 2006; Carcione 2015) related to partial saturation of gas, affecting as well the reflection and transmission coefficients of the layer as a function of offset. Seismic loss means loss of high frequencies and basically the computation of spectrograms clearly reveals this phenomenon (e.g. Castagna et al. 2003). In the literature, bright spots related to the presence of gas are identified in spectrograms with this procedure (Del Ben et al. 2011). However, according to Barnes (2013), only few cases of LFS are convincing to reveal the presence of gas. Caution is required since the presence of low frequencies may be due to other causes, such as NMO stretch, which is important at far-offset traces (Dunkin and Levin 1973; Perroud and Tygel 2004). Castagna et al. (2003) state "For every example shown, the shadow was stronger than the reservoir reflection at lower frequencies, suggesting that shadows are not necessarily a simple attenuation phenomenon because

Published online: 03 May 2016

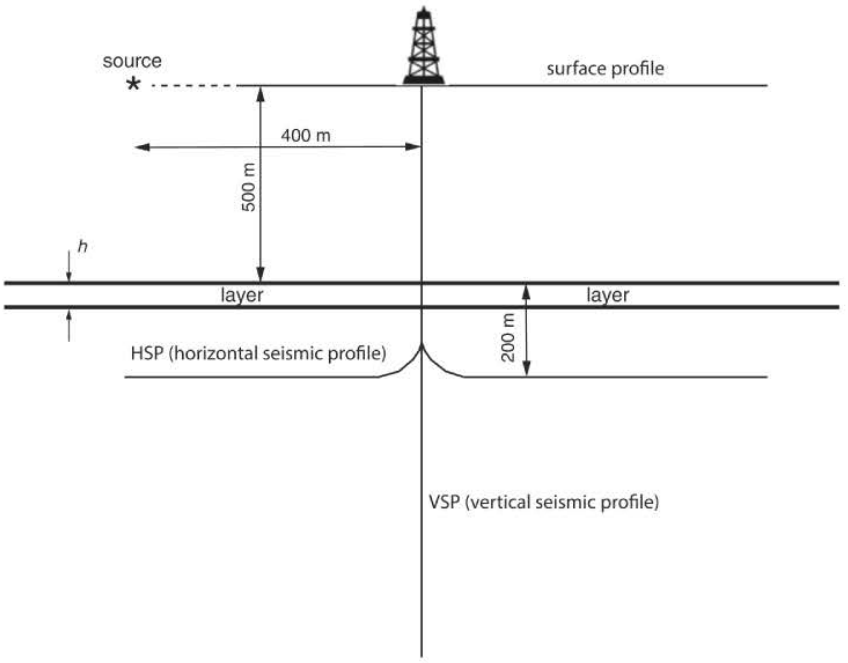

Fig. 1 Source-receivers configurations

low-frequency energy must have been added or amplified by some physical or numerical process. Attenuation alone should simply attenuate higher frequencies, not boost lower frequencies".

The case of a single interface and the influence of attenuation has been considered in Carcione et al. (1998). In this work, we compute the reflection and transmission—scattering— coefficients that characterise a layer for varying thicknesses and Q values and obtain spectrograms for different source-receivers configurations, namely surface seismic profiles, and VSP and HSP profiles (see Fig. 1). In addition, we compare the effects due to NMO stretching and intrinsic attenuation related to the LFS observed in real data after stacking. The method used here to restore the low frequencies due to NMO stretch is the algorithm proposed by Perroud and Tygel (2004). In order to study this phenomenon, we compute 2D synthetic seismograms by assuming a viscoelastic layer and varying the quality factor and thickness of the layer. The modelling algorithm is based on a spectrum of relaxation mechanisms to give a nearly constant Q factor, and the differential equations are solved in the space-time domain by using a direct method based on the Fourier pseudospectral method (e.g. Carcione 2015).

Methods and results

Let us consider a lossy layer with a P-wave velocity v_2 = 1300 m/s and density ρ_2 = 1900 kg/m^3 embedded in a background medium with v_1 = 2200 m/s, density ρ_1 = 2300 kg/m^3 and Q = 1000. The velocities correspond to the unrelaxed (high-frequency) limit. The high Q factor of the latter medium warranties that the attenuation effects are due to the layer. The viscoelastic properties are computed as indicated in Appendix A.

Figure 2 shows the representation of a plane wave through a layer, where the incidence and refraction angles are indicated, and Appendix B provides the equations to compute the P-wave scattering coefficients, which are shown in Figs. 3 and 4. Figure 3 displays the reflection (a) and transmission (b) coefficients as a function of the incidence angle for h = 30 m and three values of the quality factor, and Fig. 4 shows the coefficients for Q = 5 and three values of the layer thickness. As can be seen, low Q values (high attenuation) and varying thickness affect the scattering properties of the layer significantly. Either the reflection and transmission coefficients change by a factor of two at normal incidence for Q varying from 5 to 100 (see Fig. 3).

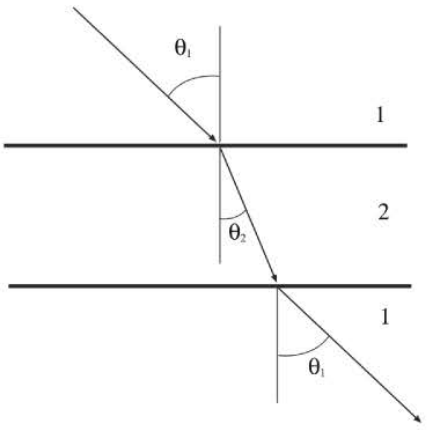

Fig. 2 Representation of a plane wave through a layer

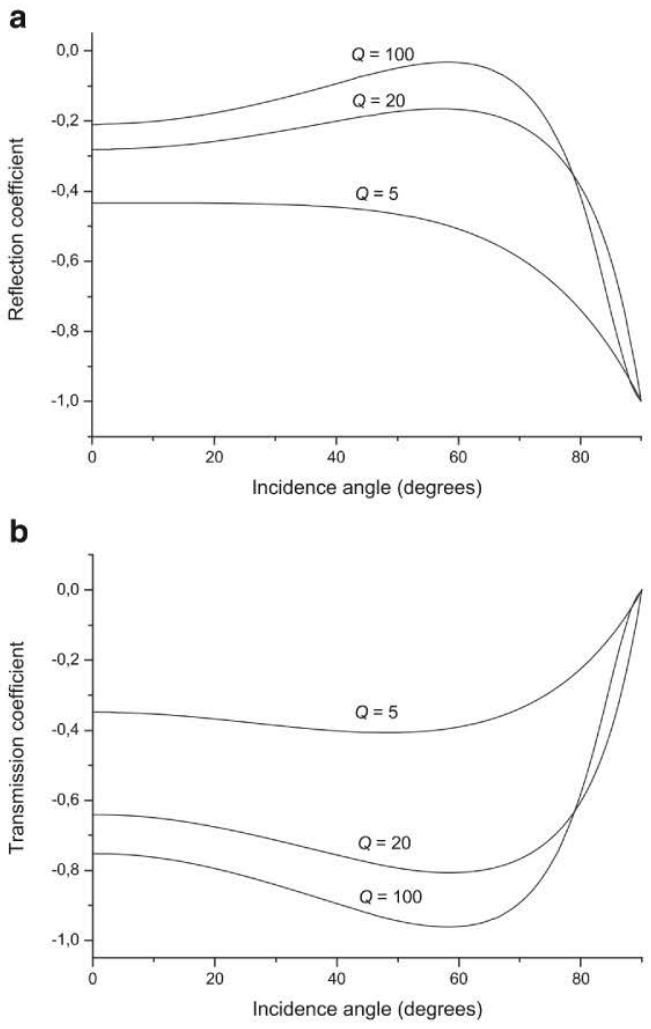

Fig. 3 Real part of the reflection (**a**) and transmission (**b**) coefficients of the layer for three Q factors, where $h = 30$ m

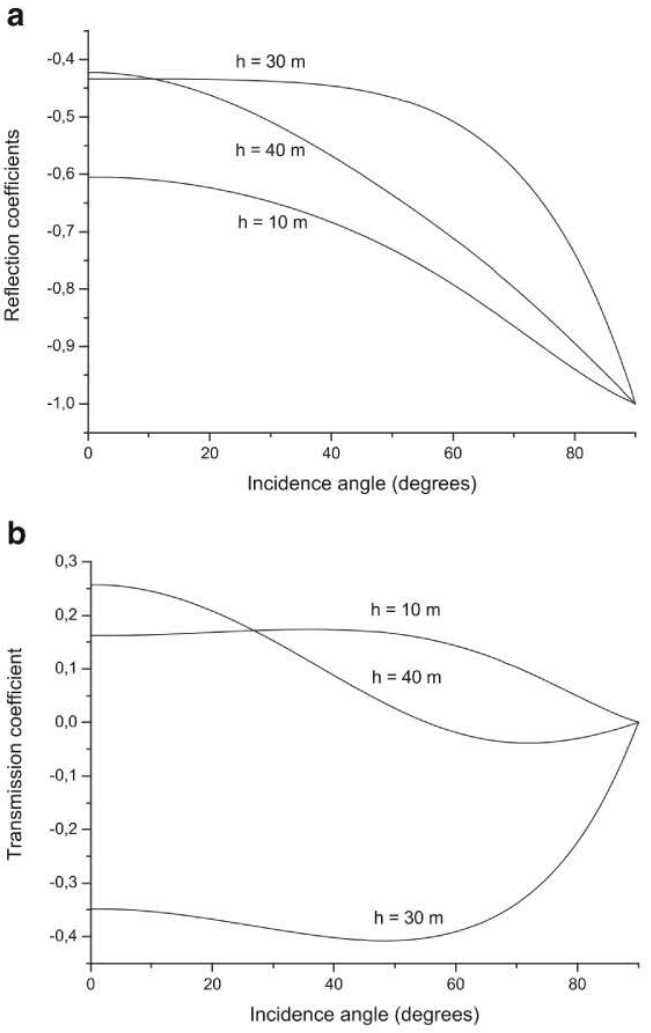

Fig. 4 Real part of the reflection (**a**) and transmission (**b**) coefficients of the layer for three thicknesses, where $Q = 5$

These calculations are essential for the interpretation of real data.

Figure 5 shows the seismograms corresponding to (a) a surface profile, (b) a VSP and (c) a HSP. The thickness of the layer is $h = 10$ m and $Q = 5$. The spectrograms are displayed in Fig. 6, where the amplitude decreases with offset mainly due to the geometrical spreading of the wavefield. The decrease in the surface profile is less pronounced than in the HSP because in the first case, the absolute value of the reflection coefficient increases with offset (see Fig. 4). The frequency bands above 500 m in the VSP correspond to the combined spectra of the direct wave and reflected event from the layer (see Marfurt and Kirlin 2001).

Figure 7 represents the spectrograms for $h = 10$ m (a), 40 m (b) and 100 m (c) corresponding to the HSP experiments with $Q = 5$ in the layer. The spectrum of each single trace is normalised to one, since in this case, we analyse the loss of high-frequency components of the signal by observing the shift to low frequencies of the centroid of the spectrum. We observe that the centroid has been shifted towards the low frequencies. This shift can be used to quantify the Q factor and the presence of fluid on the basis of a rock-physics model such as wave-induced fluid flow causing attenuation (Carcione and Picotti 2006). Spectrograms for $Q = 100$ (a) and $Q = 5$ (b) corresponding to the VSP experiments are displayed in Fig. 8, where the layer thickness is $h = 10$ m. We have represented the response below the layer, since above is the same in both cases. It is clear that the loss of amplitude in the second case is due to wave loss, even if the thickness is much smaller than the signal wavelength, which is of the order of 90 m.

The NMO correction affects the seismic event at medium and far offsets by stretching the pulse and removing high frequencies. This effect can be confused with physical attenuation. Let us consider the case $h = 10$ m and $Q = 100$ in the layer, so that the main effect is due to NMO stretch.

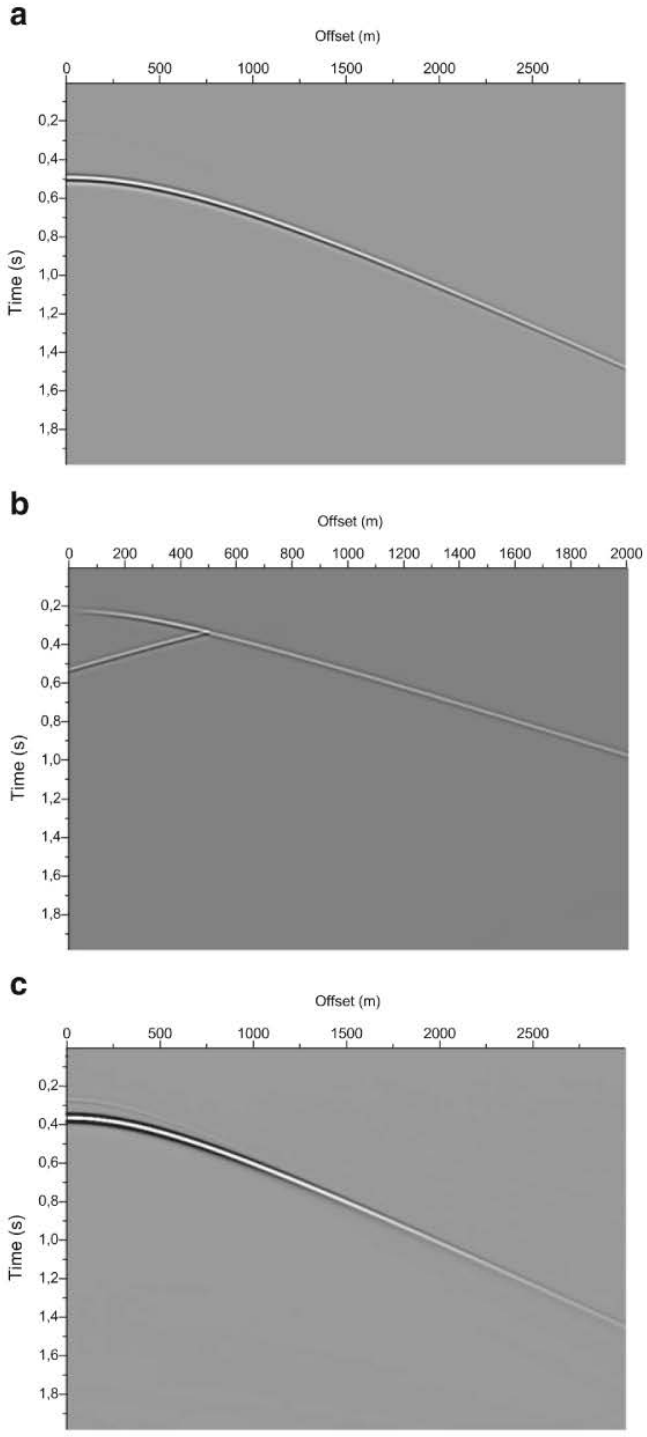

Fig. 5 Seismograms: (**a**) Surface profile, (**b**) VSP and (**c**) HSP. The thickness is $h = 10$ m and $Q = 5$

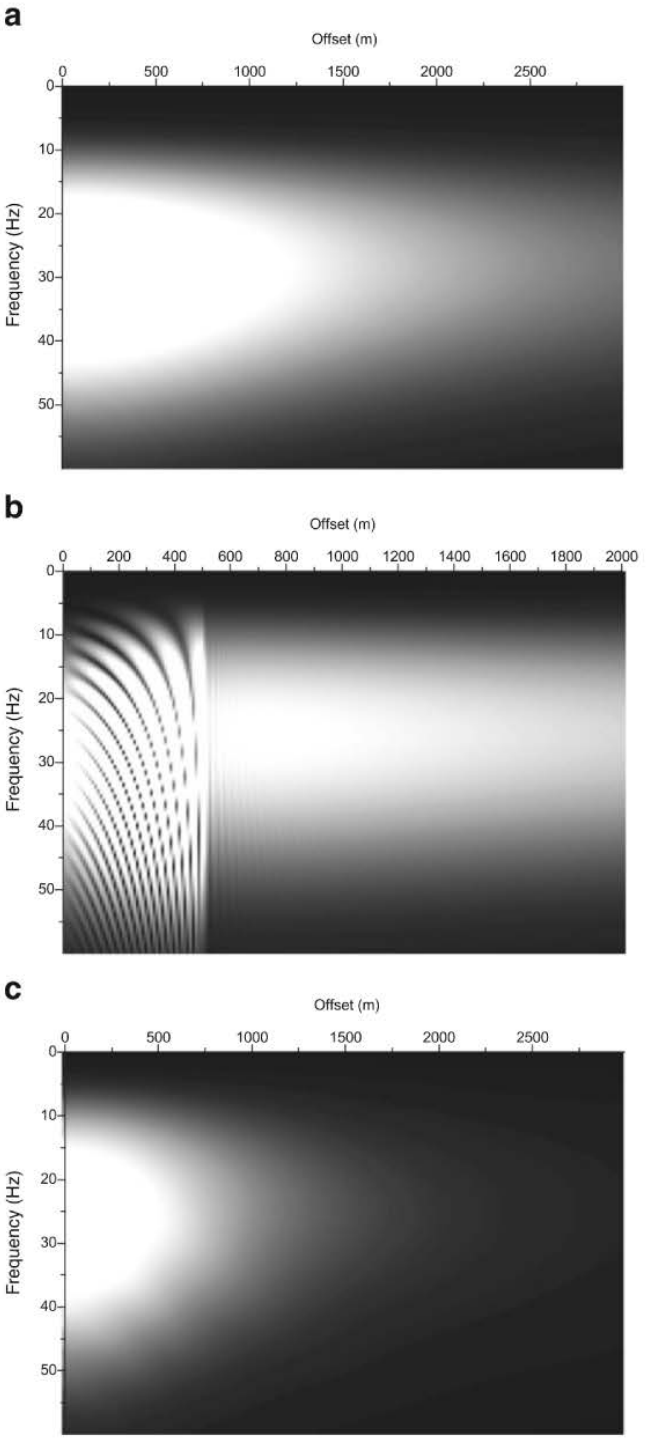

Fig. 6 Spectrogram of the reflection response (before NMO), where (**a**) Surface profile, (**b**) VSP and (**c**) HSP. The thickness is $h = 10$ m and $Q = 5$

Figure 9 shows the NMO-corrected event (a) and its frequency spectrum as a function of offset (b). The loss of frequencies with offset can be observed. NMO stretch can cause a shift of the stacked event to lower frequencies (Dunkin and Levin 1973) and therefore, stretch corrections are required to distinguish between physical attenuation and this artefact. The method used here, illustrated in Appendix C, to avoid the low frequencies due to NMO stretch, is the algorithm proposed by Perroud and Tygel (2004). We assume $\tau = 56$ ms and apply Eq. 12 with

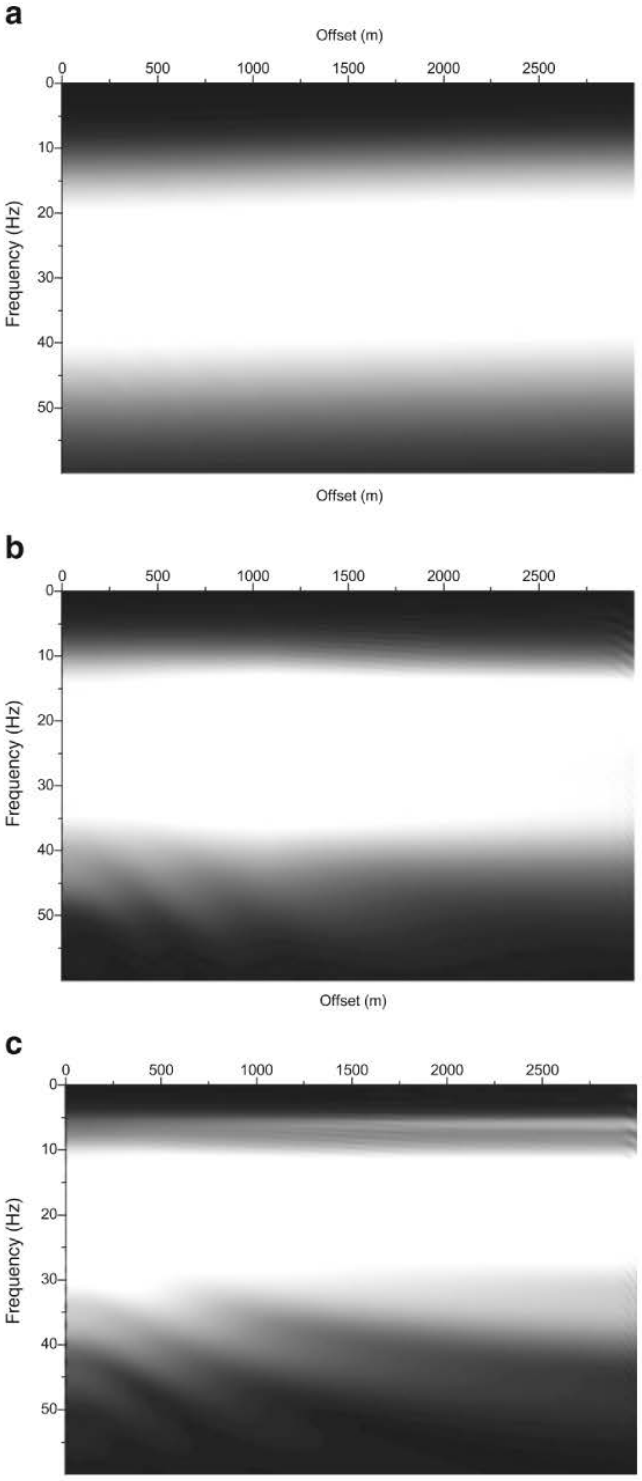

Fig. 7 Normalised spectrograms for $h = 10$ m (**a**), 40 m (**b**) and 100 m (**c**) corresponding to the HSP experiments with $Q = 5$ in the layer

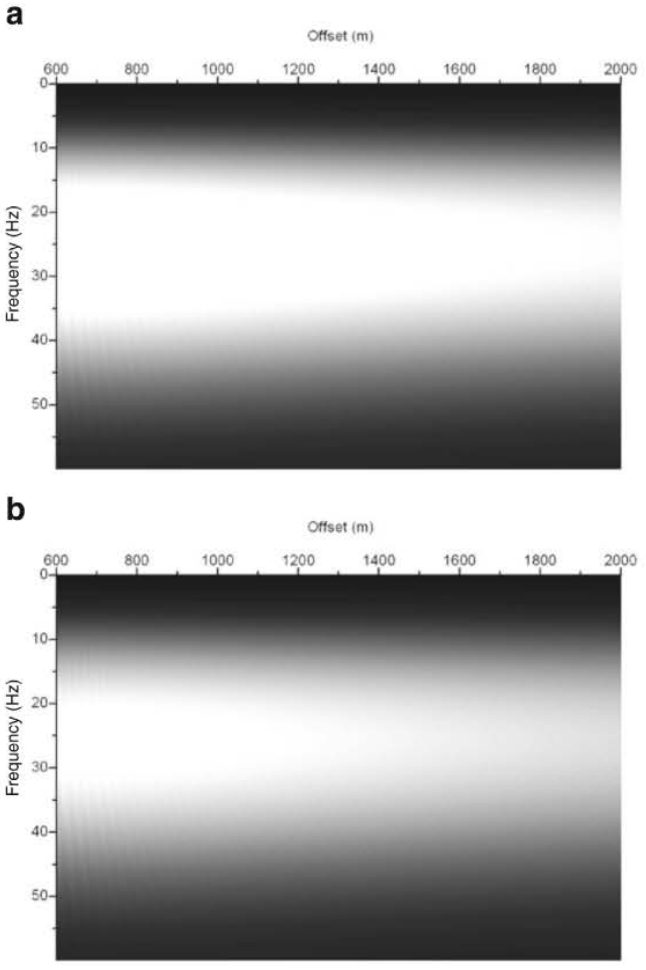

Fig. 8 Spectrograms for $Q = 100$ (**a**) and $Q = 5$ (**b**) corresponding to the VSP experiments with $h = 10$ m

$v_{NMO} = v_{RMS} + 50$ m/s. Figure 10 shows the RMS velocities (dashed line) and $v(\tau)$ (solid line) used to perform the non-stretch NMO correction. The corrected gather is represented in Fig. 11. The effectiveness of the non-stretch NMO correction can be seen in Fig. 12, where we represent the normalised amplitude spectrum of the stacked far-offset traces (2 to 3 km) corresponding to the stretch (dashed line) and non-stretch (solid line) NMO corrections. The high frequencies have been recovered. However, the loss of frequencies due to NMO can be confused with intrinsic attenuation effects as shown by comparison of Figs. 9b and 13, which corresponds to an upper half-space with $Q = 40$. It is believed that most low-frequency shadows observed in real data, related to the presence of gas (Taylor et al. 2000), are due to artificial NMO effects (Ebrom 2004).

A possible flowchart to attack the problem represented by the interpretation of a thin layer can:

1. Compute the reflection and transmission coefficients to analyse the AVO (amplitude variations with offset) characteristics of the thin layer.
2. Acquire data with source-receivers configurations other than the surface profile, which provide more information (VSP and HSP).

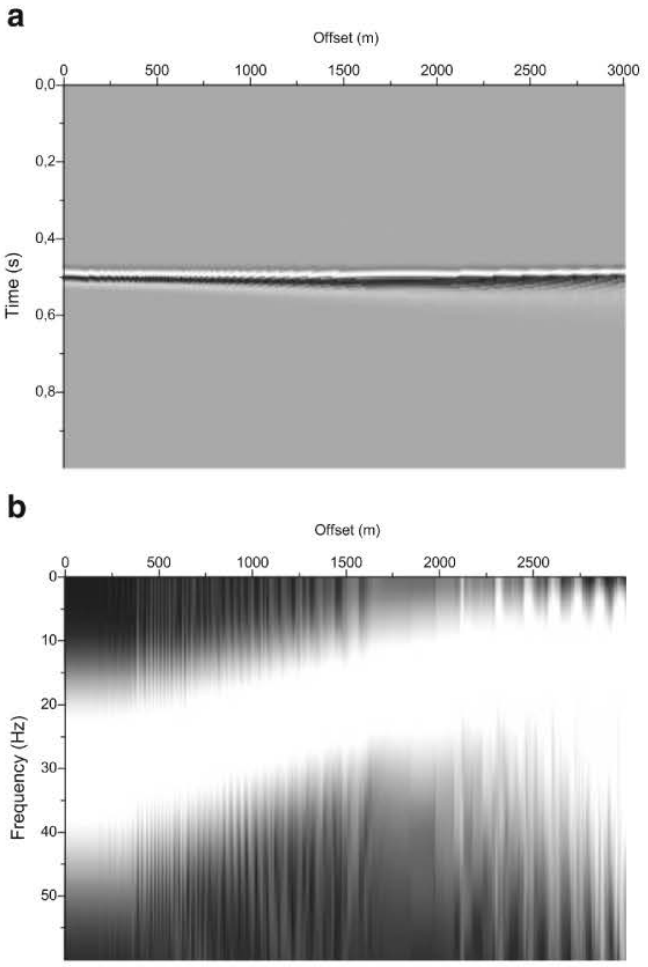

Fig. 9 NMO corrected event (**a**) and normalised spectrogram (**b**) (surface profile)

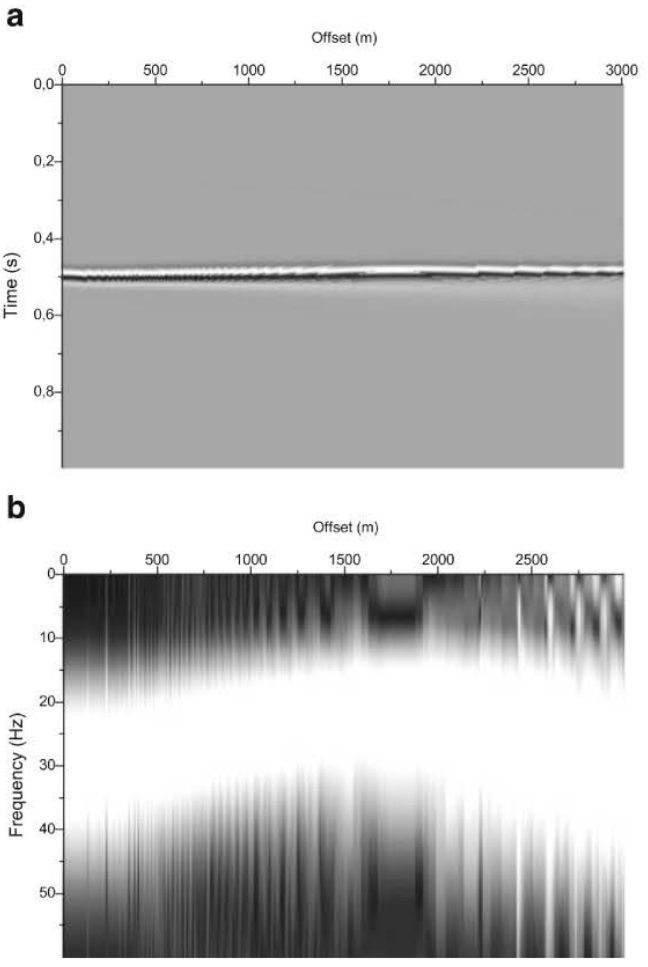

Fig. 11 Non-stretch NMO corrected event (**a**) and normalised spectrogram (**b**) (see Fig. 9)

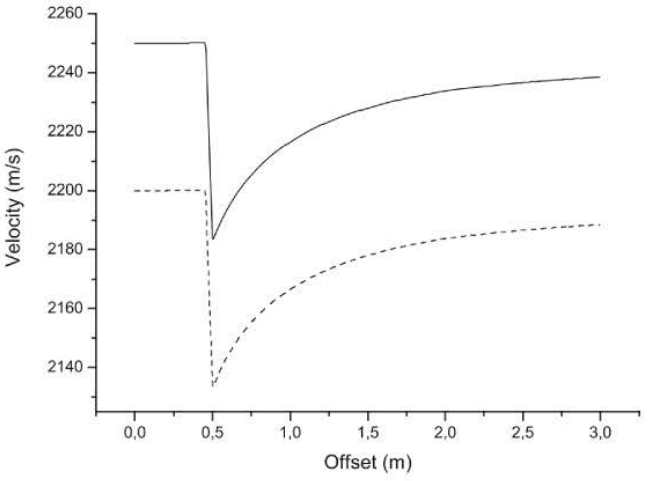

Fig. 10 RMS velocity (*dashed line*) and velocity profile used to perform the non-stretch NMO correction (*solid line*)

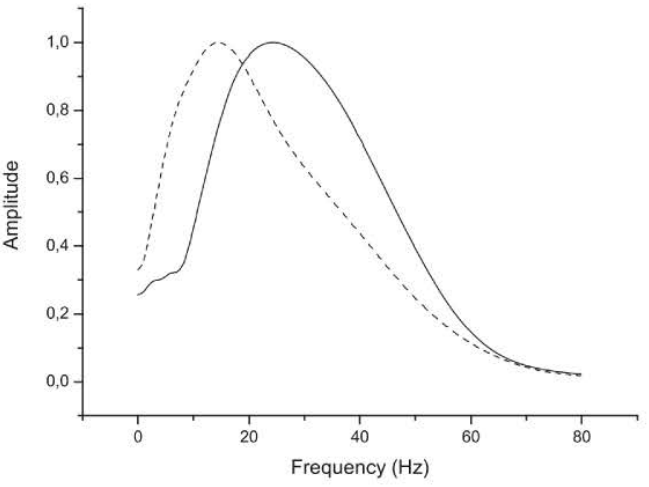

Fig. 12 Normalised amplitude spectrum of the stacked far-offset traces (2 to 3 km) corresponding to the stretch NMO correction (*dashed line*) and non-stretch NMO correction (*solid line*)

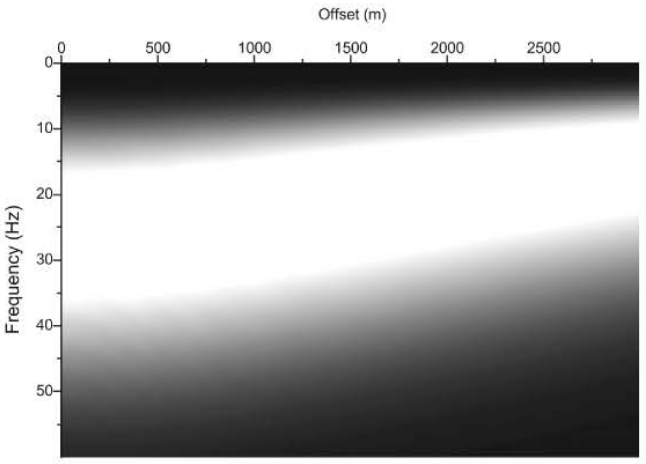

Fig. 13 Normalised spectrogram of the reflection response (before NMO), with $Q = 40$ at the upper half-space

3. Analyse the spectrograms corresponding to the different configurations to estimate the Q factor and the thickness of the thin layer, computing synthetic seismograms (and their respective spectrograms) to help the interpretation.
4. Regarding the surface profile, estimate the NMO stretch and proceed to recover the lost frequencies in order to obtain a better imaging of the thin-layer response after stacking (possible define the top and bottom of the layer). This is performed by applying the non-stretch NMO correction.
5. Use modelling experiments (synthetic seismograms) to differentiate the frequency loss due to intrinsic attenuation and NMO stretch for each specific case.

Conclusions

We have analysed the seismic attenuation effects of a relatively thin layer on different source-receiver configurations by computing the spectrograms as a function of offset. The results indicate that either the reflection or transmission coefficients change by a factor of two at normal incidence for Q varying from 5 to 100. The decrease of amplitude as a function of offset at the surface profile is less pronounced than in the horizontal profile below the layer (e.g. horizontal well) because in the first case, the absolute value of the reflection coefficient increases with offset.

The frequency bands above the layer in the VSP correspond to the combined spectra of the direct wave and reflected event from the layer. This is a phenomenon that allows one to obtain the thickness of the layer and perhaps information about the attenuation features of the medium. We will study these bands for varying Q factor in a future work. Below the layer, we observe that the centroid has been shifted towards the low frequencies. This shift can be used to quantify the Q factor and the presence of fluid on the basis of a rock-physics model of attenuation. Spectrograms for high and low Q in a 10-m layer, corresponding to the VSP experiments, indicate that the loss of amplitude in the second case is significant, even if the thickness is much smaller than the signal wavelength.

Moreover, we show that stretch NMO effects can be confused with seismic attenuation. A proper non-stretch correction is required in this case; otherwise, false conclusions can be inferred about the presence or absence of fluids, which cause high attenuation.

Appendix A: Anelasticity

The phase velocity, attenuation factor and quality factor of a viscoelastic medium are

$$c_{\mathrm{p}} = \left[\mathrm{Re}\left(\frac{1}{c}\right)\right]^{-1}, \quad \alpha = -\omega \mathrm{Im}\left(\frac{1}{c}\right) \quad \text{and} \quad Q = \frac{\mathrm{Re}(c^2)}{\mathrm{Im}(c^2)}, \tag{1}$$

respectively, where here c is the complex velocity of the P-wave, ω is the angular frequency $\omega = 2\pi f$ and "Re" and "Im" take real and imaginary parts (e.g. Carcione 2015).

We consider a constant quality factor, $\bar{Q}$, obtained with a spectrum of L Zener relaxation mechanisms, whose peak locations are equispaced in $\log \omega$ scale (see Section 2.4.6 in Carcione (2015)). We then have to find the relaxation times $\tau_{\epsilon l}$ and $\tau_{\sigma l}$ that gives an almost constant Q in a given frequency band centred at $\omega_{0m} = 1/\tau_{0m}$. This is the location of the mechanism situated at the middle of the band, which, for odd L, has the index $m = L/2 + 1$. The minimum quality factor of the L peaks is the same and is given by

$$Q_0 = \frac{\bar{Q}}{L} \sum_{l=1}^{L} \frac{2\omega_{0m}\tau_{0l}}{1 + \omega_{0m}^2 \tau_{0l}^2} \tag{2}$$

Carcione (2015), where ω_{0m} is defined below and $\omega_{0l} = 1/\tau_{0l}$ are the peak locations. Then, the relaxation times are

$$\tau_{\epsilon l} = \frac{\tau_{0l}}{Q_0}\left(\sqrt{Q_0^2+1}+1\right) \quad \text{and} \quad \tau_{\sigma l} = \frac{\tau_{0l}}{Q_0}\left(\sqrt{Q_0^2+1}-1\right). \tag{3}$$

If f_0 is the central frequency of the source wavelet, we assume that the centre peak is located at $\omega_{0m} = 2\pi f_0$.

Finally, the complex P-wave modulus is given by

$$E(\omega) = \rho c^2 = E_U \left(\sum_{l=1}^{L} \frac{\tau_{\epsilon l}}{\tau_{\sigma l}}\right)^{-1} \sum_{l=1}^{L} \frac{1 + \mathrm{i}\omega\tau_{\epsilon l}}{1 + \mathrm{i}\omega\tau_{\sigma l}} \tag{4}$$

(Carcione 2015; Eq. (2.196)), where $E_U = \rho v^2$ is the unrelaxed, high-frequency limit modulus and v is the real-valued elastic velocity. If $\omega \to \infty$, $E \to E_U$. Taking into account that $E = \rho c^2$, the quality factor is given by Eq. 1.

Appendix B: Reflection and transmission coefficients

Let us denote with 1 and 2 the background medium and layer, respectively (see Fig. 2) and consider only the P-waves. The reflection and transmission coefficients of a single layer of thickness h embedded in a homogeneous medium, corresponding to an incidence wave with angle θ_1, are

$$R = \frac{r\left[1-\exp(-\beta)\right]}{1-r^2\exp(-\beta)} \quad \text{and}$$
$$T = \frac{4Z_1Z_2\cos\theta_1\cos\theta_2}{(Z_2\cos\theta_1+Z_1\cos\theta_2)^2}\frac{\exp(-\beta/2)}{1-r^2\exp(-\beta)} \tag{5}$$

Brekhovskikh (1960), Carcione et al. (2014), respectively, where

$$\beta = 2ih\left(\frac{\omega}{v_2}\right)\cos\theta_2, \quad Z_j = \rho_j c_j, \quad j = 1,2, \tag{6}$$

$i = \sqrt{-1}$, ω is the angular frequency, c is the complex P-wave velocity, θ_2 is the refraction angle

$$r = \frac{Z_2\cos\theta_1 - Z_1\cos\theta_2}{Z_2\cos\theta_1 + Z_1\cos\theta_2}, \tag{7}$$

and Snell's law is $\sin\theta_1/c_1 = \sin\theta_2/c_2$. Here, we use the convention $\exp(i\omega t)$ for the Fourier transform. The incident wave is homogeneous, i.e. the propagation and attenuation directions coincide (e.g. Carcione 2015).

Appendix C: Correction of the NMO stretch

Dunkin and Levin (1973) have explained the stretch effect after the NMO correction. Let us assume that at a given offset, the signal before the NMO correction is $f(t)$. After the correction, the new (stretched) signal becomes

$$g(t) = f(t/a), \tag{8}$$

where a is the stretch ratio, given below. The frequency domain version of Eq. 8 is

$$G(\omega) = aF(a\omega), \tag{9}$$

where G and F are the Fourier transforms of f and g, respectively. The stretch ratio is

$$a = \frac{t}{t_0}\left(1 - \frac{x^2}{t_0 v_s^3}\left.\frac{dv_s}{dt_0}\right|_{t_0}\right)^{-1}, \tag{10}$$

where t is the uncorrected traveltime, t_0 is the corrected traveltime, x is the offset and v_s is the stacking velocity.

The correction can be performed in the frequency domain, based on Eq. 9 by restoring each frequency component ω to the right value $a\omega$ and dividing the result by a, i.e. if G is the uncorrected spectrum, we have

$$F(\omega) = \frac{1}{a}G\left(\frac{\omega}{a}\right). \tag{11}$$

Here, we use the method of Perroud and Tygel (2004). The basic processes, i.e. velocity analysis, NMO and stack, are unchanged. An extra step is required to avoid the stretch effect, the adjustment of the time-velocity function obtained from the velocity analysis.

If τ represents a time-shift since the onset of the seismic pulse, the following formula gives the adjusted NMO velocity $v(\tau)$ for an event at time $t(x)$ for offset x and NMO velocity v_{NMO} (obtained from the velocity analysis) at zero-offset time t_0:

$$v(\tau) = v_{NMO}\left(1 + \frac{2}{1+\sqrt{1+a^2}}\frac{\tau}{t_0}\right)^{-1/2}, \quad a = \frac{x}{t_0 v_{NMO}} \tag{12}$$

One can observe that $v(\tau)$ decreases when τ increases, so the NMO adjusted velocity always decreases along the seismic pulse. For relatively small τ, the decrease is quasi-linear and can therefore be described by a velocity at the beginning of the pulse, and a velocity at the end of the pulse, for the maximum τ whose value should correspond to the pulse length. We can approximate the NMO velocity by the RMS velocity, v_{RMS}. For n layers, the traveltime is

$$T = \sqrt{t_0^2 + \frac{x^2}{v_{RMS}}}, \tag{13}$$

where

$$v_{RMS} = \frac{1}{t_0}\sum_{k=1}^{n} v_k^2\tau_k, \tag{14}$$

v_k is the seismic velocity of the k layer, τ_k is the vertical two-way traveltime within layer k and $t_0 = \sum_1^n \tau_i$.

References

Barnes AE (2013) The myth of low-frequency shadows, EAGE Workshop on Seismic Attenuation. doi:10.3997/2214-4609.20131834

Brekhovskikh LM (1960) Waves in layered media. Academic Press Inc

Carcione JM (2015) Wave fields in real media theory and numerical simulation of wave propagation in anisotropic, anelastic, porous and electromagnetic media, 3rd edn. Elsevier

Carcione JM, Helle H, Zhao (1998) The effects of attenuation and anisotropy on reflection amplitude versus offset. Geophysics 63:1652–1658

Carcione JM, Grünhut V, Osella A (2014) Mathematical analogies in physics. Thin-layer wave theory. Ann Geophys 57:1–10. G0186; doi:10.4401/ag-6324

Carcione JM, Picotti S (2006) P-wave seismic attenuation by slow-wave diffusion: effects of inhomogeneous rock properties. Geophysics 71:O1–O8

Castagna JP, Sun SJ, Siegfried Rw (2003) Instantaneous spectral analysis: detection of low-frequency shadows associated with hydrocarbons. Lead Edge 22(2):120–127

Del Ben A, Forte E, Geletti R, Mocnik K, Pipan M (2011) Seismic exploration of a possible gas-reservoir in the south Apulia foreland. Boll Geof Teor Appl 52:607–623

Dunkin JW, Levin FK (1973) Effects of normal moveout on a seismic pulse. Geophysics 38:635–642

Ebrom D (2004) The low-frequency gas shadow on seismic sections. Lead Edge 23(8):772

Marfurt KJ, Kirlin RL (2001) Narrow-band spectral analysis and thin-bed tuning. Geophysics 66:1274–1283

Müller T, Gurevich B, Lebedev M (2010) Seismic wave attenuation and dispersion resulting from wave-induced flow in porous rocks—a review. Geophysics 75:A147–A164

Perroud H, Tygel M (2004) Nonstretch NMO. Geophysics 69:599–607

Taylor MH, Dillon WP, Pecher IA (2000) Trapping and migration of methane associated with the gas hydrate stability zone at the Blake Ridge Diapir: new insights from seismic data. Mar Geol 164: 79–89